Postprint version
paper published in: *Building and Environment, 46* (1), 134-143
doi:10.1016/j.buildenv.2010.07.005

The effect of a reflective underlay on the global thermal behaviour of pitched roofs.

S. Roels, M. Deurinck

K.U.Leuven, Department of Civil Engineering, Division of Building Physics, Kasteelpark Arenberg, B-3001 Heverlee, Belgium

Abstract: The influence of the emissivity of a roof underlay on the global thermal behaviour of sloped roofs is investigated. Five well insulated pitched roofs have been constructed in a test building. The five roofs have a south-west and north-east oriented pitch and differ in long wave emissivity of the underlay. All roofs are equipped with thermocouples and heat fluxes sensors to evaluate the thermal response of the roofs to the climatic conditions. Both summer and winter conditions have been measured. In addition to the in situ evaluation, a laboratory experiment was set-up to evaluate the influence of the emissivity of the underlay on the summer behaviour of a sloped roof under fixed boundary conditions. With thermocouples and heat flux sensors at different heights in the roof the effect of the reflective foil on the heat gain to the inside could be evaluated. The measured data are compared with a simple numerical model that accounts for the buoyancy effects in the ventilated cavity between tiles and underlay.
Laboratory experiments and simulations revealed that a low emissivity of the underlay decreases the heat gain to the indoor environment, but that due to the thermal stack flow in the air cavity underneath the tiles, the advantage of a reflective foil mainly plays a role in the bottom part of the roof. In the in situ measurements it was found that workmanship, airtightness and wind and thermal stack effects are much more important and disturb the possible benefits of using a reflective underlay.

1. Introduction

Since the first energy crisis in the 1970s, energy regulations for buildings led to a systematic increase of the thermal resistance of the building envelope. Apart from a higher insulation layer thickness, other possibilities have been put forward to increase the thermal performances of building components. One of them is the use of reflective layers, which is mainly popular in (sloped) roof constructions. These building components play indeed an important role in the overall heat losses in wintertime and heat gains in summertime. To reduce solar irradiation and high heat gains through the roof in hot climates, coatings are often used to cover the exterior side of the roof component, leading to a significant effect on reducing the unwanted heat gains in summer conditions [e.g. 1-2]. Apart from coating the outer surface, so-called low-e barriers are used e.g. to reduce the heat transfer in attics [3,4] or inside building components to decrease the radiant heat exchange in air gaps [5-8]. Mainly in light weight constructions a growing use of

reflective foils can be noticed. And, if advertising materials can be trusted, the importance of reflective foils on the overall thermal behaviour of building components can't be underrated. In literature, the advantages of the reflective barrier are often investigated numerically or experimentally with laboratory experiments [5-7]. In the laboratory, building components can be studied at well controlled, constant boundary conditions. This provides useful information about partial aspects. However, former experiments have shown that the real hygrothermal behaviour of insulated envelope parts is strongly determined by the unstable components of the outside climate: wind, driving rain, solar radiation, supercooling... [9-11]. All typical transient aspects, difficult to simulate in a laboratory. Therefore, field testing is an essential step to assess the behaviour of building components in its overall complexity, taking into account all aspects that appear in a real building under real climatic conditions.

In this study, the effect of a reflective underlay on the global thermal behaviour of pitched roofs is investigated. Four types of underlay with varying emissivity have been studied both under laboratory and real climatic conditions. The paper starts with a description of the tested roof systems. Then the laboratory set-up is presented. In these experiments the effect of the emissivity of the underlay on the heat transfer through the roof is analysed for simplified stationary summer conditions. The measured data are compared with a simple numerical model that accounts for the buoyancy effects in the ventilated cavity between tiles and underlay. With the numerical model the impact of the emissivity of the underlay on the stationary heat fluxes through the roof can be estimated, assuming that wind effects can be neglected. The obtained results are expressed as a reduction of the heat gains through the roof due to the reflectivity of the underlay and can be seen as the most optimal reduction that can be achieved with a reflective underlay for the given set-up. In the last part, the field data as measured on the roofs installed in the test building are analysed. In contrast to the laboratory experiments, the boundary conditions are no longer steady state and wind will play an important role in the overall thermal behaviour.

2. Tested roof systems

The tested roof systems are so-called compact roofs, consisting of, from outside to inside: concrete tiles, ventilated cavity (50 mm), Tyvek® underlay, mineral fibre insulation between the rafters (145 mm), air and vapour retarder, non ventilated cavity (25 mm) and paint coated gypsum board. The configuration of all roofs is identically, but the emissivity of the underlay surface facing the ventilated cavity underneath the tiles varies. The Tyvek Homewrap® with an emissivity of 0.47 acts as reference. In addition two more reflective foils (emissivity 0.13 and 0.2) and one less reflective foil (emissivity 0.7) have been tested. The emissivity of the underlay types was determined in the laboratory of Dupont de Nemours, Luxembourg.

Note that common standards are not very clear on how the emissivity of the underlay can be taken into account in the theoretical thermal resistance of the roofs. According to ISO 6946 [12] the air layer between tiles and underlay has to be considered as well ventilated and hence the

thermal resistance of the air layer and tiles is disregarded, but instead the value of the external surface resistance is taken equal to the internal surface resistance. If the design values of the surface resistance are used two times the internal surface resistance has to be added to the thermal resistance of the roof component. In this case the total thermal resistance of all roof systems is the same – regardless of the emissivity of the underlay – and counts up to 5.06 m²K/W. Only if the surface resistance is calculated according to the specific prescriptions in Annex A of ISO 6946 the effect of the emissivity can be explicitly taken into account. In this case the surface resistance is given by

$$R_s = \frac{1}{h_r + h_c} \tag{1}$$

with $h_r=4e\sigma T_m^3$ and h_c depending on the direction of the heat flow. In this way the surface resistance can only be calculated for specific boundary conditions. For winter conditions (heat losses through the roof; h_c=5.0 W/m²K; T_m=273 K) the external resistance will vary between 0.122 m²K/W (e=0.7) and 0.179 m²K/W (e=0.13). For summer conditions (heat gains through the roof; h_c=0.7 W/m²K; T_m=333 K) the difference is larger and varies between 0.152 m²K/W (e=0.7) and 0.559 m²K/W (e=0.13).

For the field tests, pitched roofs were built in the VLIET test building of the Laboratory of Building Physics at the K.U.Leuven (see Figure 1). The test building has the possibility to study building envelope parts exposed to real weather conditions and to evaluate their energy efficiency, hygric behaviour and durability. In total five roofs have been constructed in pairs on the NE and SW oriented pitch. Figure 2 shows a global scheme of the roof set-up.To make the test parts representative for real envelope parts, the measuring bays of the test building are sufficiently large. The width of each roof is 1.8 meter and each pitch measures approximately five meter along the roof slope. The four types of underlay have been used, and two roof configurations have been constructed with an outer underlay emissivity of 0.7. The difference between both was the fact that one of them was made as airtight as possible by folding the underlay towards the inside and by carefully sticking this overlap at the inside. Table 1 gives an overview of the different roof assemblies.

For the laboratory tests, a mock-up of the roofs as installed in the VLIET test building has been built. Only one pitch of the roof has been constructed, with a total length of 3 meter and a slope of 45°. The width of the mock-up measures only 60 cm, corresponding to the width of two concrete tiles.

Both the roofs for the field testing as for the laboratory experiments were equipped with thermocouples and heat flux sensors to evaluate the thermal response of the roofs to the imposed boundary conditions. The global configuration with sensor assembly is illustrated in Figure 2. Heat flow sensors are placed at the interior side of the gypsum board and at the outside of the mineral wool. Thermocouples are placed on the surface of each layer, so that temperature

profiles and the heat flow resistance of specific layers can be captured. Both temperatures and heat flows are measured at three heights in order to detect possible air flow effects. In addition, the roofs in the test building have been equipped with humidity sensors and air tubes that can be coupled to an air pressure difference sensor to deliver more information about the local humidity and air pressure distribution in the cavities. Temperatures, heat fluxes and relative humidity are measured automatically and continuously by a computerised datalogger system.

3. Laboratory experiments

3.1.Experimental set-up

The laboratory experiments are primarily intended to evaluate the effect of the emissivity of the underlay on the summer behaviour of a sloped roof. The roof assembly of the laboratory mock-up is exactly the same as in the VLIET test-building, but the set-up is designed in such a way that the tiles and battens can easily be removed to change the underlay. In this way, one set-up can be used to measure successively different types of underlay. Stationary summer conditions are realized by heating up the outer surface of the tiles with IR-bulbs. The inside of the roof is exposed to the inside conditions of the laboratory (19°C and 50% RH). The same conditions apply for the air that enters and rises in the ventilated cavity between tiles and underlay. Figure 3 shows a global scheme of the laboratory set-up. Figures 4 show some pictures of the set-up in the laboratory.

To analyse the thermal response of the roofs under the given boundary conditions, thermocouples and heat flux sensors were installed in the bottom part of the roof (at 0.5 m of the eave), in the middle of the roof (1.5 m of eave and ridge) and in the top part of the roof (at 0.5 m of the ridge). The thermocouples were installed in the middle of the cross section at outer and inner layers, in the middle of the ventilated cavity and at each interface. Heat flux sensors were installed between underlay and insulation and at the backside of the gypsum board. The four types of underlay have been measured. For each underlay, the measurements run for one to two days. This showed to be long enough to get stationary conditions. As an example Figure 5 shows the evolution of the temperatures during the test at the different positions in the middle of the reference roof with the Tyvek Homewrap® as underlay. Analysis of all data was based on the measured mean values of the temperatures and heat fluxes under stationary conditions (see indicated period on Figure 5).

3.2.Analysis of the measured data

Figure 6 plots the measured temperature profiles at the three positions in the roof for the different types of underlay. Comparing the three figures makes the buoyancy effect in the ventilated cavity clearly visible. The temperature in the cavity and the temperature of the underlay are much lower at the bottom position than at the top of the cavity. The cold air enters the cavity at the eave and rises to the ridge while heating up. As a result, also the underlay heats up from

bottom to top. Also the effect of the emissivity is clearly visible. A lower emissivity of the underlay results in a higher temperature gradient over the cavity. Correspondingly, the temperature gradient over the insulation reduces when lowering the emissivity of the underlay and so will the heat flow to the inside. The temperature differences between the different types of underlay is however limited, compared to the global temperature rise of the underlay with the height.

Since the temperature of the underlay strongly varies along the height of the roof, also the heat gain to the inside will vary along the height of the roof. This makes it difficult to quantify the efficiency of the reflective underlay in reducing the heat gains in summer conditions. The overall efficiency will be dependent on the roof set-up (length and slope of the roof, width of the cavity, closure of the tiles,...) and on the outside boundary conditions (incident solar radiation, outside air temperature). Furthermore, it has to be kept in mind that these laboratory experiments are steady state experiments and that wind effects are neglected. Nevertheless it is worth to quantify the reduction of the heat gains by applying a reflective underlay for the current set-up.

Figure 7 plots the temperature of the underlay at the three positions as a function of the emissivity of the underlay. In Figure 8 the interior heat flux (measured at the back side of the gypsum board) is given as a function of the emissivity of the underlay. Both temperature and heat gains are strongly dependent on the position in the roof, but the influence of the emissivity on temperature and heat flux is clear. Though, it can be seen that the effect mainly plays if the emissivity of the underlay is very low (< 0.25).

If the plain white Tyvek Homewrap® with an emissivity of 0.47 is taken as the reference, the relative reduction/increase in heat gain can be calculated for the different positions. Table 2 gives the absolute values of the measured heat fluxes and the relative decrease compared to the reference roof. Comparing the absolute values, it can be seen that the difference in heat gain to the inside between the reflective underlay types and the reference case diminish along the height of the roof. At the same time, the absolute heat flux to the inside increases. As a result large differences in relative decrease are found along the height of the roof. Taking the value at the middle position as a kind of averaged value, a decrease in heat gain of 17.5% and 6.8% is found for the underlay with outer emissivity of 0.13 and 0.2 respectively. Increasing the emissivity of the underlay (emissivity of 0.7), on the other hand, hardly increases the heat fluxes to the inside.

3.3.Numerical simulations

If no wind effects are taken into account and assuming that air can only enter the ventilated cavity at the eave and leave at the ridge, the laboratory set-up can be simulated with a simple numerical model. To do so, the ventilated cavity between tiles and underlay has been subdivided in ten control volumes. For each volume the heat balance equations can be written. The unknown temperatures are the cavity surface temperatures of tiles and underlay, the interior and outer surface temperature and the air temperature in the cavity. In the cavity, heat transport is possible

from tiles to underlay by conduction, convection and radiation. At the same time, the cavity air will heat up and flow upwards due to buoyancy effects. Friction between air and cavity surfaces will slow down the air flow. In addition to the heat balance equation for each control volume, the global balance of thermal stack and friction closes the set of equations:

$$3460\left[\frac{H_{sp}}{T_{in}} - \int_z \frac{dz}{T_{sp}(z)}\right] = \frac{Ga^2}{2\rho_a b_{sp}^2}\left[f\frac{H_{sp}}{2b_{sp}} + \xi_{sp}\right] \qquad (2)$$

with H_{sp} the height of the cavity (m), T_{in} the temperature of air entering the cavity (taken equal to the laboratory temperature of 292K), $T_{sp}(z)$ the temperature of the cavity in the volume where z is situated (K), Ga the air flow (kg/m.s), ρ_a the air density (kg/m^3), b_{sp} the width of the cavity (m), ξ_{sp} the local air flow resistance factor (taken as 0.5 for the inlet and 1 for the outlet) and f the friction coefficient of the cavity boundary (-). In Equation (2) a cavity length of 1 meter is assumed and the air inlet surface is taken equal to the cavity surface: one meter multiplied with the width of the cavity.

The heating up of the tiles by the IR-bulbs is implemented as a heat flux at the outer surface of 600 W/m² except for the first and second control volume element for which respectively 50 and 75% of this value is taken. This assumption corresponds to the fact that the radiation of the different IR-bulbs will overlap more in the middle of the set-up than at the borders.

Figure 9 shows the ten control volumes of the roof and the temperature nodes which are calculated for each volume. If the air flow in the cavity is known, the set of heat balance equations of the first control volume can be solved to determine the five unknown temperatures (surface temperatures in the cavity, interior and outer surface temperature and cavity air temperature) by taking the laboratory temperature as inlet temperature of the cavity. Once the heat balance equations of the first control volume are solved, the cavity temperature of the first control volume can be taken as inlet temperature for the second control volume and the heat balance equations of the second control volume can be solved. This way all the temperatures of the different control volumes can be consecutively calculated. With these temperatures, the global thermal stack equation (Eq. 2) can be updated to determine a new air flow. The updated air flow is used to resolve the heat balance equations of the control volumes. After a few iterations the model is converged.

Figure 10a compares the simulated temperature profiles of the underlay along the height of the roof with the measured values for the different types of underlay. Figure 10b does the same for the heat flux at the interior surface. Nevertheless the simplifications, it can be seen that the numerical model predicts the measured data fairly well. The underlay temperatures are overestimated with 5 to 10 K, the heat gains to the inside slightly underestimated. But the global tendencies are well predicted and the relative differences between the thermal behaviour of the different types of underlay correspond very well to the measured data.

Given the reasonable agreement between laboratory measurements and numerical predictions, the model may be used to estimate the impact of the reflective underlay on the heat gains / heat losses through the roof for more general summer and winter conditions and for other values of the emissivity of the underlay. Note however, that the model remains stationary (only the steady state behaviour of the roof can be analysed for fixed boundary conditions) and that no wind effects are taken into account.

First a summer day is analysed with a high solar radiation on the roof (1000 W/m²). The outside temperature and hence the inlet temperature of the cavity between tiles and underlay is taken at 25°C. At the inside an interior temperature of 20°C is assumed. The inside and outside surface coefficients are taken as respectively 8 and 25 W/m²K. The roof configuration is kept similar to the roof tested in the laboratory experiment: the same assembly is used and only one slope with a total length of 3 meter positioned under 45° is investigated. The thermal response of the roof is calculated for an emissivity of the underlay varying from 0.1 to 0.9 in steps of 0.1. A value of 0.47 is calculated as well as reference case, corresponding to the Tyvek Homewrap®.

Figure 11 plots the heat flux (heat gains) to the inside as calculated in the middle of the roof (1.5 m from eave and ridge) as a function of the emissivity of the underlay. A similar graph as the one obtained for the laboratory experiments is found (see Figure 8). The heat gains to the inside reduce when the underlay becomes more reflective, but the effect is most pronounced when the emissivity of the underlay is very low. This can also clearly be noted when analysing Table 3 which gives the absolute values of the calculated heat fluxes in the middle of the roof and the relative decrease compared to the reference roof. Compared to the reference roof a very reflective underlay (emissivity of 0.1) reduces the heat gains to the inside with 10.5%, while on the contrary increasing the emissivity to 0.9 only results in an increase of the heat gains with 2.2%.

In addition to the summer day, the numerical model has been used also to analyse the thermal behaviour of the roof systems with reflective underlay for cold clear winter nights. However, due to supercooling the temperature of the tiles will drop below the outside air temperature and no – or a small downwards instead of upwards – air flow in the cavity is observed. As a result, the effect of the emissivity of the underlay comes back to the theoretically calculated values for a (non-ventilated) cavity.

It is important to keep in mind that the simulations and laboratory experiments are dealing with stationary boundary conditions and that no wind effects are taken into account. Both effects may disturb the ‘theoretical’ thermal behaviour of the roofs. Furthermore, the experiments have been performed with new underlay foils. Aging and dusting of the underlay may increase its emissivity and reduce the predicted effect. In the next section the effect of the emissivity of the underlay is investigated under real climatic conditions by in situ measurements on the roofs constructed in the VLIET test-building.

4. In-situ measurements

The roofs were constructed in spring 2009. The measurement campaign ran from June 2009 until February 2010, so that both summer and winter conditions could be studied. The thermal response of the roofs is completely different in summer and winter period. While in winter period the heat flow remains continuously a heat loss for the building, in summer conditions the sign of the heat flow may change during the day. Therefore, the analysis of the measured data for both periods will be discussed separately.

4.1.Summer conditions

Under summer conditions, great temperature differences may occur in a roof construction during the period of a single day: high temperatures around noon due to incident solar radiation and low temperatures at night due to supercooling. Therefore, the temperatures and heat fluxes along the roof are no longer steady state, but vary strongly within the period of one day. As a result, looking at averaged values is not possible, so no thermal resistances or thermal transmittances can be calculated from the summer data. But, the response of the roofs can be analysed based on a short period of time. To reduce the influence of wind effects and to have maximum influence of the solar radiation, the behaviour of the roofs on a warm and sunny day with hardly any wind (Augusts 19th 2009) is analysed in detail (Table 4). In this analysis, only the south-west oriented pitches are considered, since they undergo the highest daily temperature difference. It is expected that the influence of the different types of underlay will be more visible for these roofs in comparison with the north-east oriented pitches.

Figure 12 shows as an example the daily variation of the temperatures along the middle position for the air tight roof with the highest emissivity of the underlay. One can clearly see the location of the insulation between the underlay and air and vapour retarder. The tiles and underlay follow the dynamic fluctuations of the outside boundary conditions, while the gypsum board and inside cavity react quite stable due to the indoor climate system of the Vliet test building. Although the maximum outdoor air temperature is only around 30°C, the temperatures of the tiles and underlay easily reach values of 60°C and more due to the incident solar radiation. To compare the fluctuating in-situ data with the stationary laboratory experiment, a short period of the day is analysed separately. For each roof, the 10-min values between 15:00 and 16:00 of August 19th 2009 are averaged. Figure 13 plots the averaged temperature profiles between 15:00 and 16:00 at the three positions of each roof (at the top, which is at 1 m of the ridge, in the middle of the roof and at the bottom position, which is at 1 m of the eave). Although the laboratory experiments showed a clear difference between the different types of underlay, it is difficult to draw conclusions from the in-situ measurements. The different types of underlay do not lead to distinct differences in measured temperature profiles. While all roofs act very similar at the bottom position, more pronounced differences are found at the middle and top of the roof. At these positions, slightly higher underlay temperatures are found when the underlay has a higher emissivity. The tendency however is very weak. Also the buoyancy effect that was clearly visible in the laboratory experiment, can hardly be detected in the in-situ data. The temperature of the outer side of the underlay is only slightly lower at the bottom position. When thermal stack

occurs, one would expect at the inlet of a cavity temperatures that are near the outdoor air temperature. The fact that this is not the case in the in-situ roof cavities, might be explained by the presence of the rain gutter at the bottom of the roof and the detailing of the ridge. The specific detailing at the rain gutter and ridge can lead to a high air flow resistance at the inlet and outlet of the cavity, by which the thermal stack flow is reduced.

The inside summer comfort is mainly correlated to the inner heat flux. To be able to compare the fluctuating in-situ data with the steady-state laboratory experiment, again a short period of the day, where the inner heat fluxes can be assumed to be nearly stationary, is analysed separately. A phase shift occurs between the opposed outside boundary conditions and the measured heat fluxes on the inside. Therefore, a different time period is chosen to average the 10-min-values of the inner heat fluxes: the 10-min-values of the heat fluxes are averaged from 16:00 until 18:00 - instead of 15:00 until 16:00 for the temperatures. The averaged inner heat fluxes are plotted in function of the emissivity of the underlay in Figure 14. Contradictory to the laboratory experiments, no clear conclusions can be drawn about the influence of the emissivity of the underlay on the inner heat fluxes. At the top position, the roof with lowest underlay emissivity even shows the highest inner heat flux.

Considering that the laboratory experiments showed a very good correlation between the emissivity of the underlay and the thermal performance of the roof under (stationary) summer conditions, it is remarkable that the analysis of the field data show very little to no correlation. One explanation could be the aging and dusting of the underlay by which the emissivities of the underlay become quite similar to each other. Also, wind effects can disturb the heat transfer through the roofs. Furthermore, one can presume that small differences in execution could play an unexpected role on the thermal behaviour. In the laboratory, the different experiments were configured on the same mock-up. Only the tiles and underlay were removed to change to a different type of underlay, while the rest of the mock-up and measurement equipment stayed untouched. In theory, the roofs in the test-building also have the same configuration (except from the type of underlay), while, in practice, small differences in execution are inevitable. To check whether variations in thermal resistance occur, the thermal resistance of the different roofs is calculated in the next section based on the measured data for winter conditions

4.2.Winter conditions

In winter conditions, the measured surface temperature and heat fluxes can be used to calculate the in situ thermal resistance values. The traditional thermal performance indicators such as the U-factor (W/(m²K) and the thermal resistance or R-value (m²K/W) are however only defined for pure heat conduction, while the measured values are also influenced by air looping, wind washing and dynamic effects. Therefore the concept ‘local apparent thermal resistance R’ is introduced as a measure for the thermal performance of the roof. It is calculated from the surface temperatures (inside gypsum board and inside underlay) and the inner heat flux and gives an “apparent” thermal resistance R, not to be confused with the theoretical thermal resistance.

Two calculation methods have been used to determine the in situ apparent R-values: linear regression and averaging. The linear regression method is based on the fact that, if only heat conduction would occur, the temperature difference $\Delta\theta$ over and the heat flux *q* through the roof should be proportional to each other: the larger the temperature difference, the larger the heat flux. This proportionality can be described by a linear function: when all measured daily averaged heat fluxes q (W/m^2) are plotted against the measured daily averaged temperature difference $\Delta\theta$ (°C) between the inside of the gypsum board and the inside of the underlay a linear regression can be applied, in which the thermal resistance R determines the slope:

$$q = \frac{1}{R} \cdot \Delta\theta + \varepsilon \qquad \left[\frac{W}{m^2}\right] \tag{3}$$

In Equation (3) ε is a constant error term, accounting for the fact that the heat transfer through the roof differs from pure heat conduction.

In the averaging technique, the local apparent thermal resistance is calculated by summing up all measured daily averaged temperature differences and dividing them by the sum of all measured daily averaged heat fluxess:

$$R_{local,app} = \frac{\sum \Delta\theta}{\sum q} \tag{4}$$

Figure 15 compares the results of both methods for all ten pitches based on the daily averaged data for December 2009 and January 2010. As a reference also the theoretical R-value of the roofs is given. Note that the apparent thermal resistance is calculated from underlay to gypsum board and that the ventilated air gap underneath the tiles and hence, the emissivity of the underlay, is not taken into account. This means that for all configurations the same value is expected. Based on figure 15 it can be concluded that the local apparent R-values of all roofs are in the same order of magnitude and that they correspond well with the theoretical value. However, small differences occur, both between the different roofs and between the results of both determination methods. Although these differences are small, they are at least in the same order of magnitude as the effect of the emissivity of the underlay on the thermal resistance of the ventilated air gap underneath the tiles.

4.3.Dusting of the underlay

The laboratory set-up and the numerical model depicted that the effect of a reflective underlay mainly plays if the emissivity of the underlay is very low ($e < 0.25$). At these low emissivities, small changes in the emissivity have a large impact on the heat flux (see Figures 8 and 11). Therefore, it is important to know the current emissivity of the underlay of the in-situ roofs since these emissivities might have increased over time due to dusting. After the measuring campaign, samples of the underlay were collected from each roof of the VLIET test building. The tiles were

locally removed and a piece of the underlay was carefully cut out. Samples were collected at the SW and NE-side and at the top and bottom position of the pitch. The emissivity of these samples was measured in the laboratory of Dupont de Nemours, Luxembourg. Figure 16 plots the measured emissivity of the in situ samples against the initial emissivity. The measurements indicate that the metalized underlays cannot maintain their low initial emissivity. The most reflective foil even shows emissivities around twice the initial value after two years of in situ exposure.

This dusting and aging of the underlay, together with the small variations in the local apparent thermal resistance, may explain the lack of tendency between the emissivity of the underlay and the in situ measured thermal response of the roofs.

5. Conclusions

The effect of the emissivity of the underlay on the global thermal response of sloped roofs has been investigated by well controlled laboratory experiments, field testing and a numerical model. The small scale laboratory set-up was built to analyse the effect on heat gains through a roof for simplified stationary boundary conditions. The measurements showed that the emissivity of the underlay has a clear influence on the thermal response of the roof. Both the air temperature of the cavity between tiles and underlay and the temperature of the underlay itself was significantly lower when an underlay with low emissivity was used. Also the buoyancy effects in the cavity were clearly measurable. Cold (laboratory) air enters the cavity between tiles and underlay and heats up while flowing to the ridge. As a result the heat gains to the inside vary along the height of the roof, but at all positions the heat gain to the inside was clearly correlated to the emissivity of the underlay. A lower emissivity reduced the heat gains to the inside. Quantifying the effect is however difficult, since it is dependent on the position in the roof and the configuration of the set-up. For the current configuration, a decrease in heat gain in the middle of the roof with respectively 17.5% and 6.8% was found for the highly reflective underlay (e=0.13 and 0.2 respectively) compared to the Tyvek homewrap®, which was taken as reference case (e=0.47). When an underlay with a higher emissivity was used the effect was much less pronounced.

The laboratory experiments have been simulated with a simple numerical model that subdivides the roof along its height in ten different elements. Solving the heat balance equation for each element in combination with the global thermal stack equation for the cavity between tiles and underlay makes it possible to simulate the laboratory experiments. A good correspondence between measurements and simulations was found. When using the developed numerical model for more general outdoor boundary conditions similar results as in the laboratory experiments were found: the heat gains to the inside reduce when the underlay becomes more reflective, but the effect is most pronounced when the emissivity of the underlay is very low.

Compared to the laboratory experiments, the analysis of the in situ measured data does not show a distinct relation between the emissivity of the underlay and the heat transfer through the roofs.

Plotting the inner heat fluxes as a function of the underlay emissivity, does not reveal any correlation. Also the buoyancy effect is nearly detected in the roof, which can probably be explained by the high inlet air friction at the rain gutter and the detailing of the ridge. One possible explanation for the fact that very little to no correlation is found between the emissivity of the underlay and the thermal performance of the roof could be aging and dusting of the underlay, since the laboratory experiments showed that the influence of the emissivity plays only a role for very low emissivities. Furthermore, analysis of the winter data showed that although all roofs in the VLIET test building have the same configuration and perform in good agreement with the expected theoretical R-value, small differences are found in the apparent thermal resistance values. Nevertheless these differences are small, they are in the same order of magnitude as the effect of the emissivity of the underlay on the thermal resistance of the ventilated air gap underneath the tiles.

References

[1] Levinson R, Akbari H, Reilly JC. Cooler tile-roofed buildings with near-infrared-reflective non-white coatings. Building and Environment 2007; 42:2591-2605.

[2] Suercke H, Peterson EL, Selby N. Effect of roof solar reflectance on the building heat gain in a hot climate. Energy and Buildings 2008; 40: 2224-2235.

[3] Winiarski DW, O'Neil DL. A quasi-steady-state model of attic heat transfer with radiant barriers. Energy and Buildings 1996; 24: 183-194.

[4] Medina MA. On the performance of radiant barriers in combination with different attic insulation levels. Energy and Buildings 2000; 33: 31-40.

[5] Michels C, Lamberts R, Güths S. Theoretical/experimental comparison of heat flux reduction in roofs achieved through the use of reflective thermal insulators. Energy and Buildings 2008; 40:438-444.

[6] Uvslokk S, Arnesen H. Thermal insulation performance of reflective material layers in well insulated timber frame structures. In: Rode C, editor. Proceedings of the 8th Symposium on Building Physics in the Nordic Countries, Report R-189, Dept. Of Civil Engineering, Technical University of Denmark, Kgs. Lingby, Denmark, 2008, p. 1-8.

[7] Chami N, Zoughaib A. Modelling the solar fraction of roof systems: study of the role of radiant barriers and traditional insulation. In: Bayazit NT et al, editors. Energy efficiency and new approaches. Istanbul Technical University, 2009, p. 295-300.

[8] Baldini G. A methodology for experimental evaluations of low-e barriers thermal properties: field tests and comparison with theoretical models. Building and Environment 2010; 45:1016-1024.

[9] Hens H, Janssens A. Heat and moisture response of vented and compact cathedral ceilings: a test house evaluation. ASHRAE Transactions 1999;105(1):837–50

[10] Künzel H. Simultaneous heat and moisture transfer in building components. One- and two-dimensional calculation using simple parameters. PhD-thesis, Universität Stuttgart, Germany; 1994.

[11] Hens H, Janssens A, Zheng R. Zinc roofs: an evaluation based on test house measurements. Building and Environment 2003; 38, p. 795 – 806.
[12] ISO 6946 Building components and building elements – Thermal resistance and thermal transmittance – Calculation method. ISO; 1996.

Tables

Table 1. Roof assembly in the VLIET test building

Emissivity of underlay	0.13	0.70	0.70	0.20	0.47
Airtight closure of underlay at eave	no	No	yes	no	no

Table 2. Measured heat fluxes [W/m²] and relative decrease [%] compared to the reference roof for bottom (B), middle (M) and top (T) position

	heat flux to inside [W/m^2]			relative decrease [%]		
emissivity	B	M	T	B	M	T
0.13	1.94	8.29	10.67	54.2%	17.5%	17.6%
0.2	2.41	9.36	12.06	43.2%	6.8%	6.9%
0.47	4.24	10.05	12.96	0.0%	0.0%	0.0%
0.7	4.26	10.27	12.59	-0.5%	-2.2%	2.9%

Table 3. Calculated heat fluxes [W/m²] and relative decrease [%] compared to the reference roof for summer day with a high solar radiation on the roof

emissivity	heat flux to inside [W/m^2]	relative decrease [%]
0.10	8.14	10.5%
0.20	8.64	5.1%
0.30	8.88	2.4%
0.40	9.03	0.8%
0.47 (reference)	9.10	0.0%
0.5	9.12	-0.2%
0.6	9.19	-1.0%
0.7	9.23	-1.4%
0.8	9.27	-1.9%
0.9	9.30	-2.2%

Table 4. Outside weather conditions on August 19th 2009.

	Aver.	Max.	Min.
Air temperature (°C)	22.3	32.4	12.6
Wind speed (m/s)	0.83	2.57	0.27
Horizontal solar radiation kW/m²)	0.26	0.76	0.00

Figure Captions.

Figure 1. View on the test building from the SW-side; the measuring bays with the pitched roof constructions are clearly visible.

Figure 2. Global configuration of the roofs with the sensor assembly indicated on the left part: the temperatures and heat fluxes are measured at three heights along each roof.

Figure 3. Global scheme of the laboratory set-up to analyse the effects of the emissivity of the underlay on the heat gain through the roof for summer conditions.

Figure 4. Pictures of the laboratory set-up to analyse the effects of the emissivity of the underlay on the heat gain through the roof for summer conditions.

Figure 5. Evolution of the temperatures at the middle positions in the reference roof. Stationary conditions were achieved within 3 to 4 hours after switching on the IR-bulbs.

Figuur 6. Temperature profiles at the bottom, middle and top position in the roofs. A lower emissivity of the underlay results in a higher temperature gradient over the ventilated cavity.

Figure 7. Measured underlay temperature plotted as a function of the emissivity of the underlay.

Figure 8. Measured interior heat fluxes plotted as a function of the emissivity of the underlay.

Figure 9. Control volume model for the sloped roofs. The red dots correspond to unknown nodes, for which the heat balance equations are solved. The white dots correspond to boundary values. The inset shows one control volume element which can be solved when the air flow in the cavity is assumed to be known.

Figure 10. Comparison of the measured (coloured dots) and simulated (continuous lines) underlay temperatures (a) and heat gains to the inside (b) along the roof set-up for the different types of underlay

Figure 11. Calculated interior heat fluxes plotted as a function of the emissivity of the underlay for a summer day with a high solar radiation on the roof.

Figure 12. Temperature profile of the SW-oriented, airtight roof with an underlay emissivity of 0.7 – August 19th 2009.

Figure 13. Temperature profiles at the top, middle and bottom position in the roofs based on the averaged 10-min values between 15:00 and 16:00 on August 19th 2009.

Figure 1.

Figure 2.

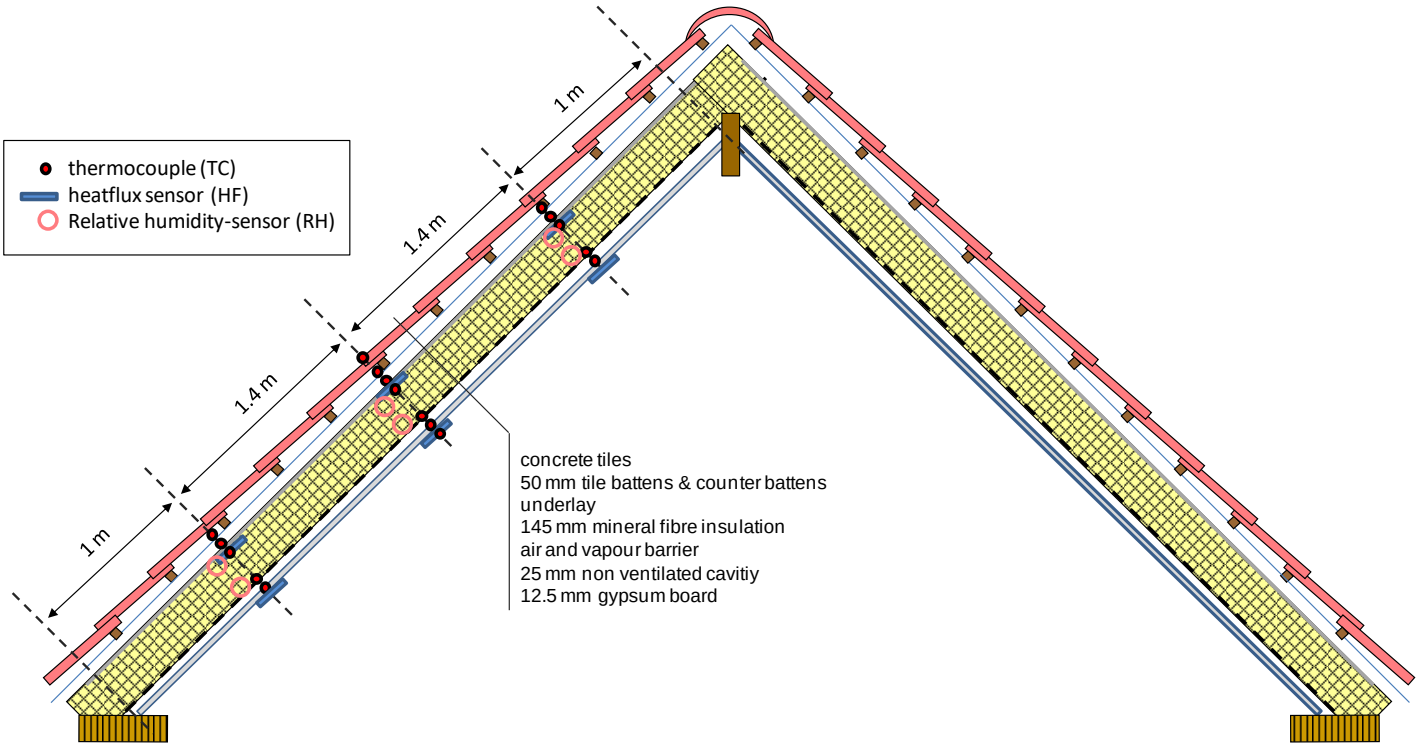
thermocouple (TC)
heatflux sensor (HF)
Relative humidity-sensor (RH)
1 m
1.4 m
1.4 m
1 m
concrete tiles
50 mm tile battens & counter battens
underlay
145 mm mineral fibre insulation
air and vapour barrier
25 mm non ventilated cavitiy
12.5 mm gypsum board

Figuur 3.

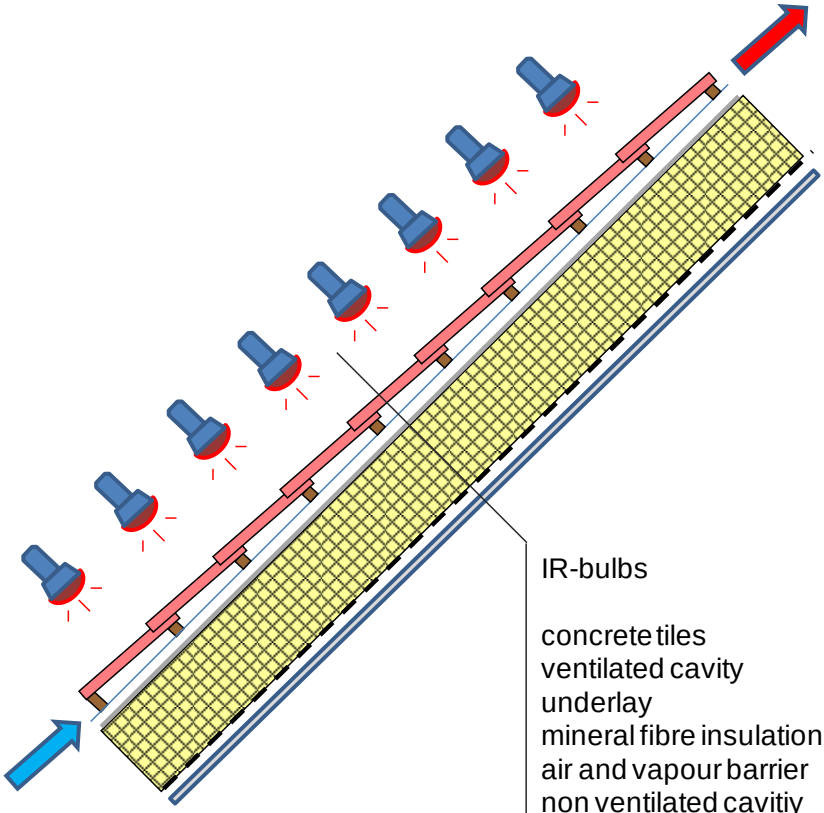

longitudinal section

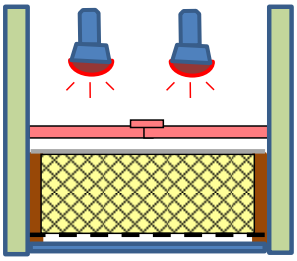

cross-section

Figuur 4.

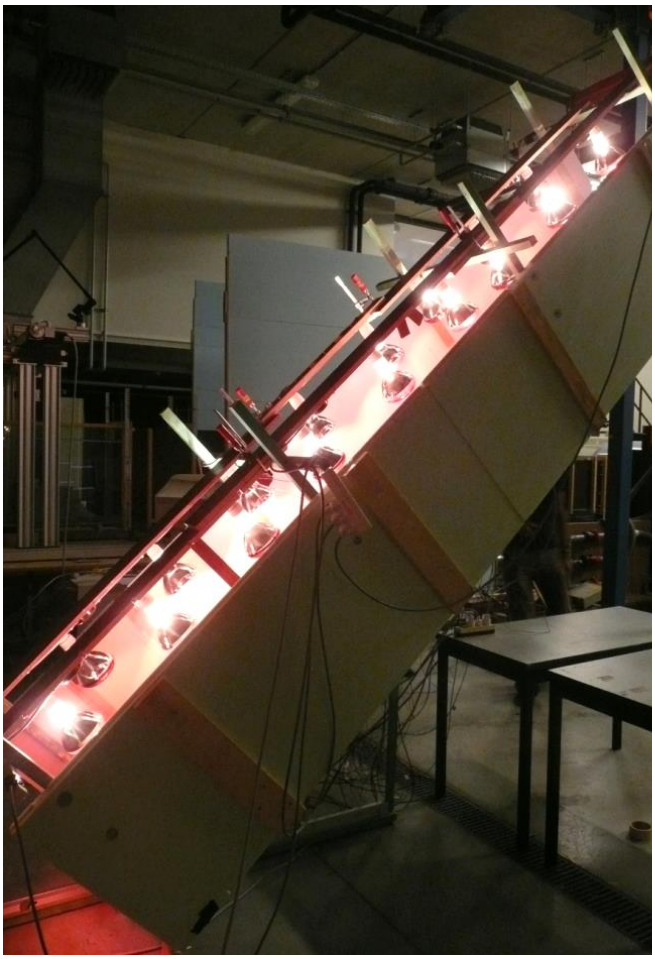

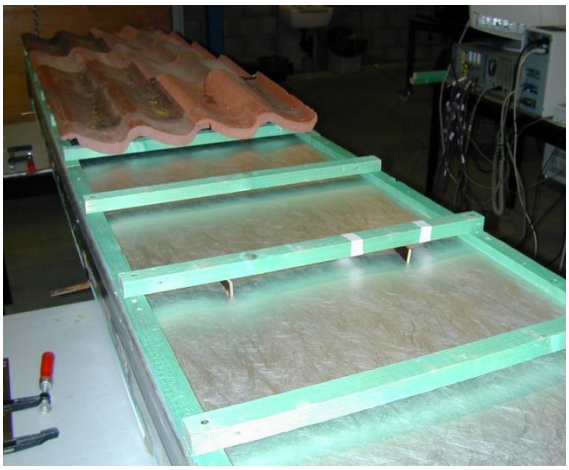

Figure 5.

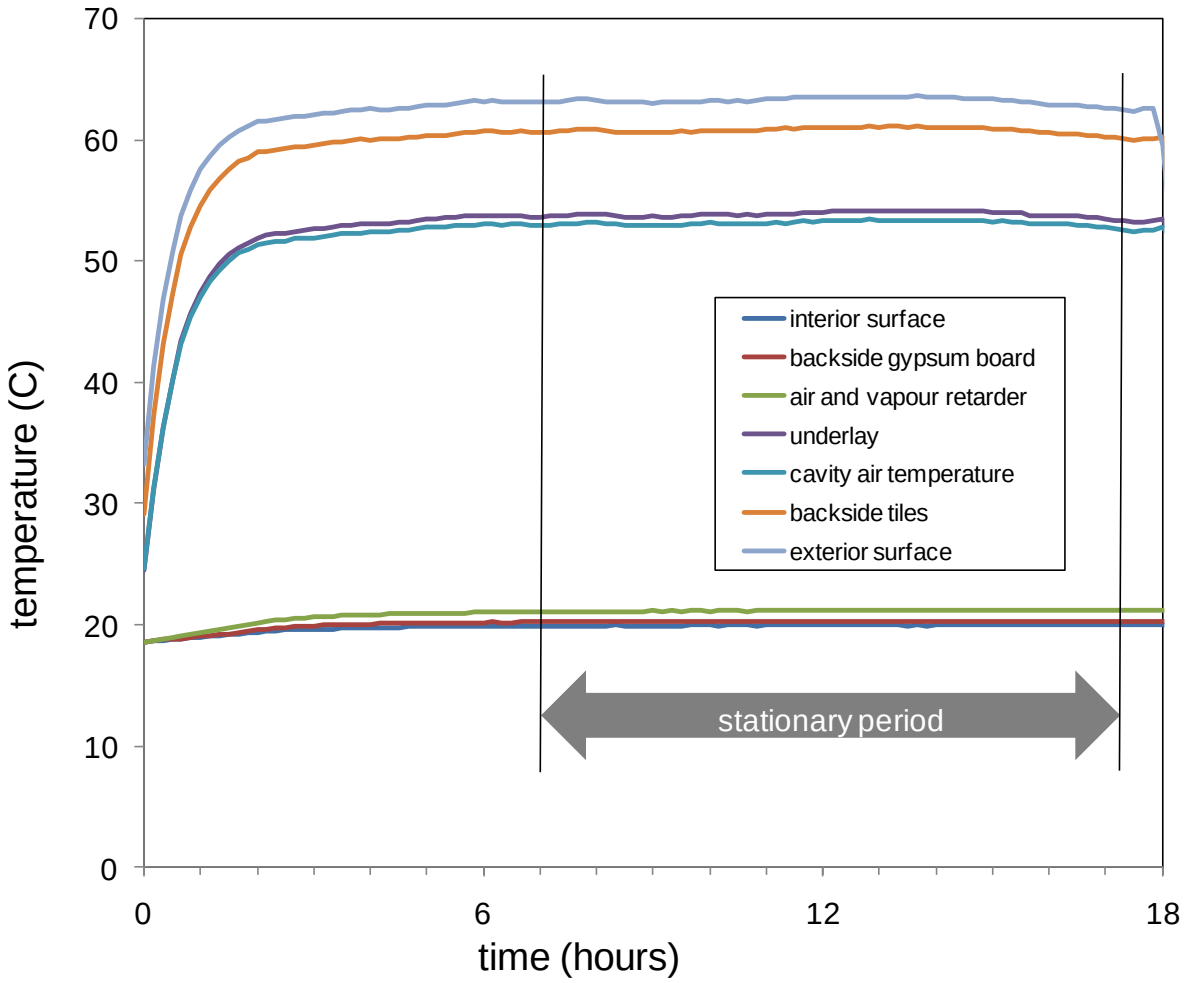
70
60
50
40
30
20
10
0
temperature (C)
0
6
12
18
time (hours)
interior surface
backside gypsum board
air and vapour retarder
underlay
cavity air temperature
backside tiles
exterior surface
stationary period

Figure 6.

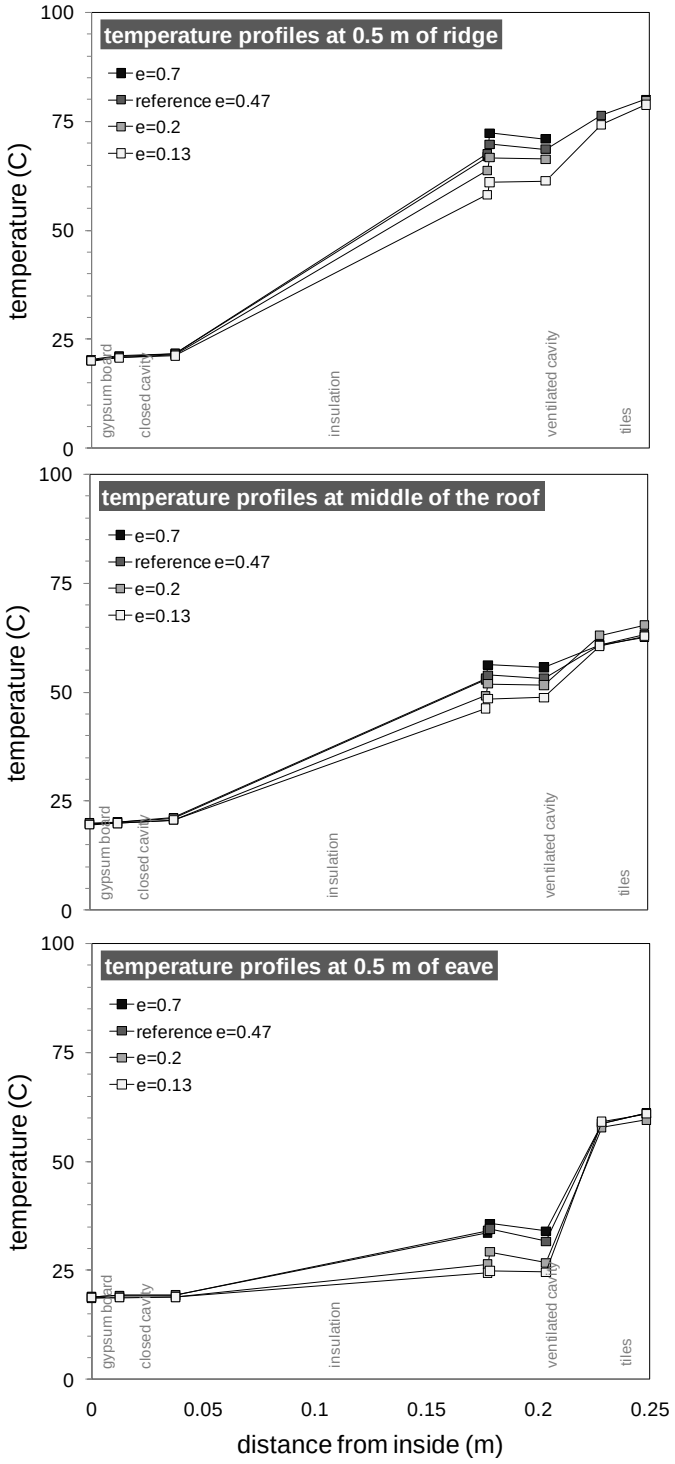
temperature profiles at 0.5 m of ridge
e=0.7
reference e=0.47
e=0.2
e=0.13
temperature (C)
100
75
50
25
0
gypsum board
closed cavity
insulation
ventilated cavity
tiles
temperature profiles at middle of the roof
e=0.7
reference e=0.47
e=0.2
e=0.13
temperature (C)
100
75
50
25
0
gypsum board
closed cavity
insulation
ventilated cavity
tiles
temperature profiles at 0.5 m of eave
e=0.7
reference e=0.47
e=0.2
e=0.13
temperature (C)
100
75
50
25
0
gypsum board
closed cavity
insulation
ventilated cavity
tiles
0
0.05
0.1
0.15
0.2
0.25
distance from inside (m)

Figure 7.

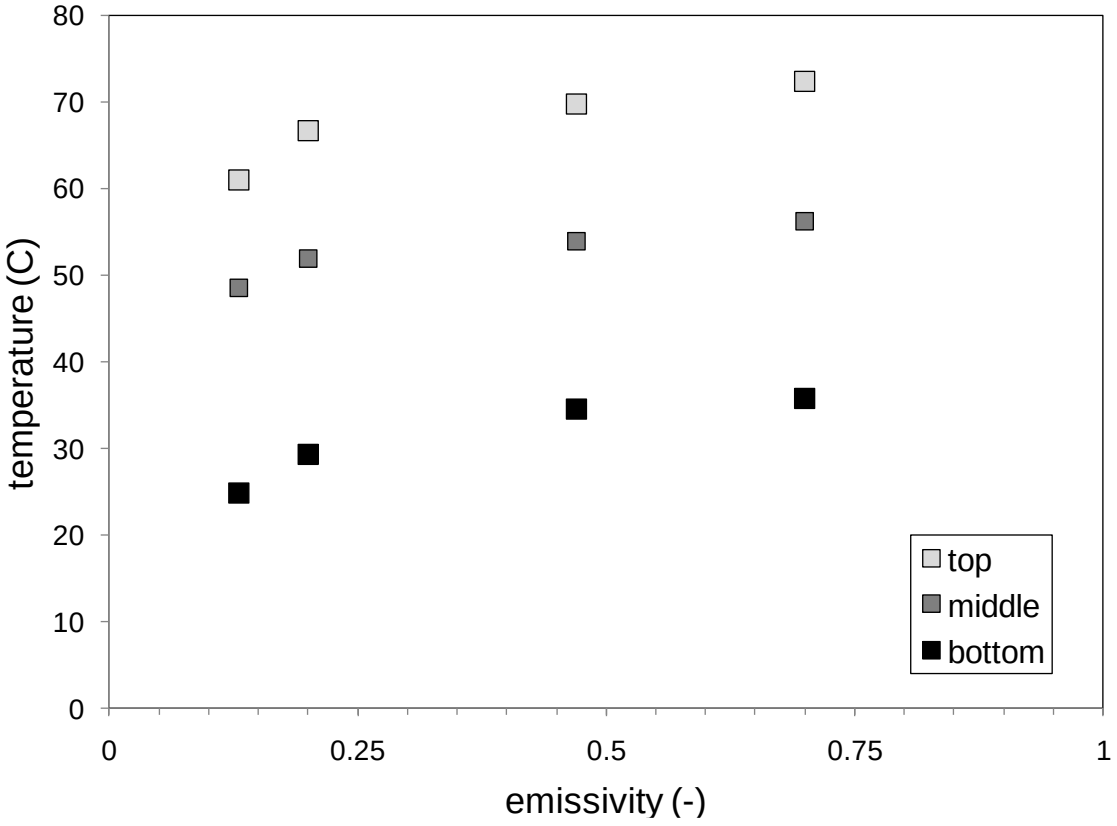
80
70
60
50
40
30
20
10
0
temperature (C)
0
0.25
0.5
0.75
1
emissivity (-)
top
middle
bottom

Figure 8.

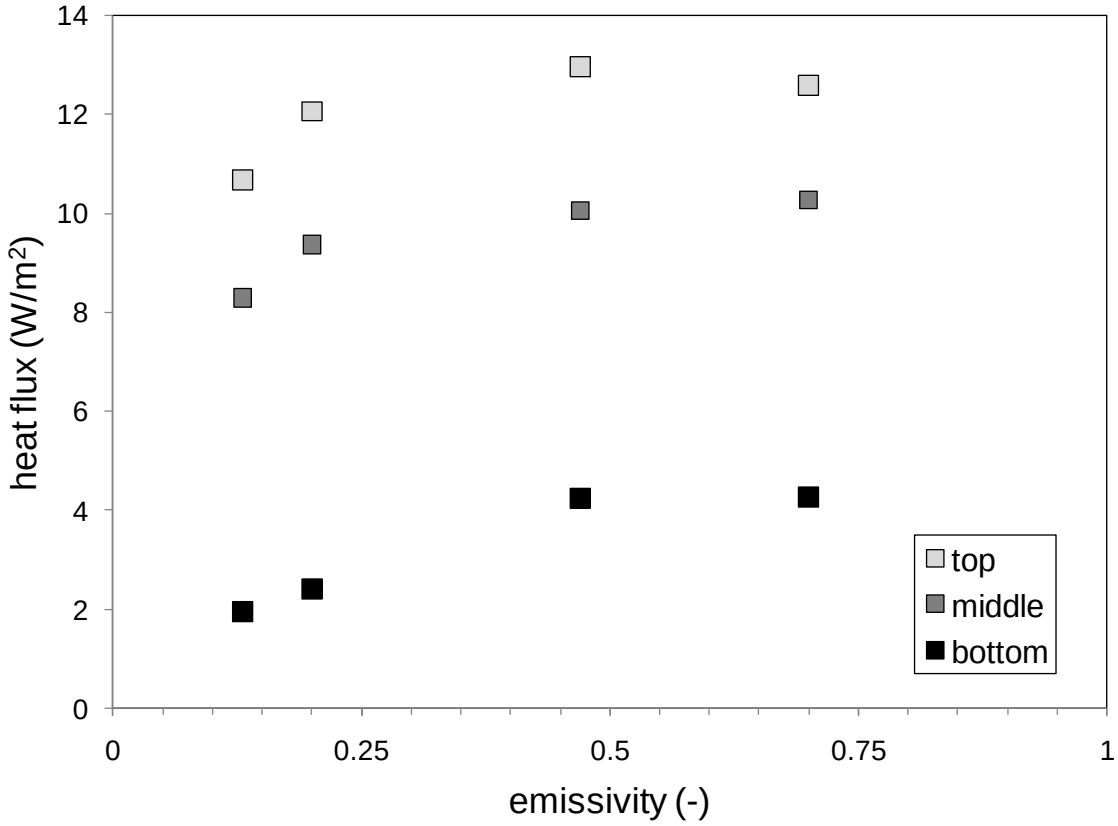
14
12
10
8
6
4
2
0
heat flux (W/m2)
0
0.25
0.5
0.75
1
emissivity (-)
top
middle
bottom

Figure 9.

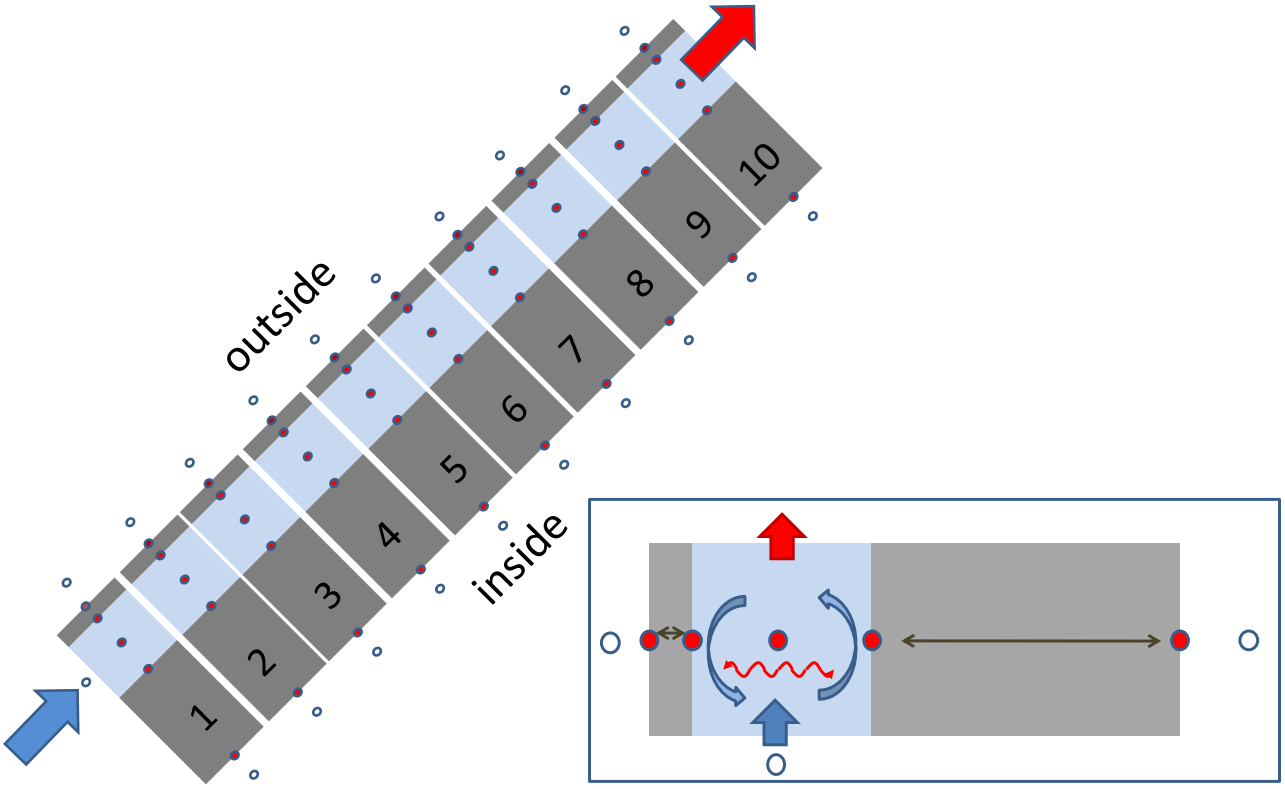

Figuur 10

(a)

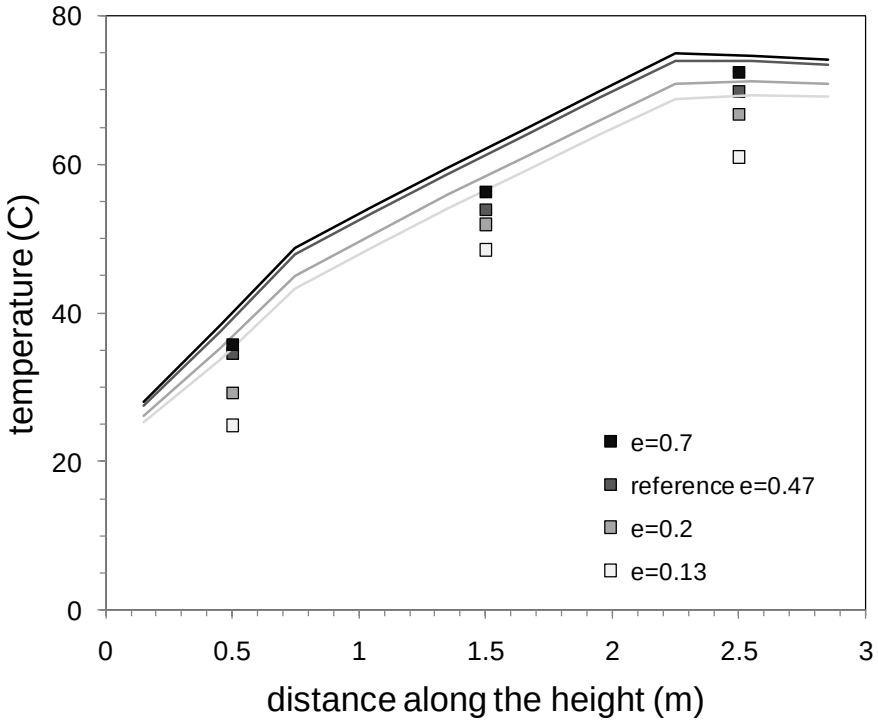
80
60
40
20
0
temperature (C)
0
0.5
1
1.5
2
2.5
3
distance along the height (m)
e=0.7
reference e=0.47
e=0.2
e=0.13

(b)

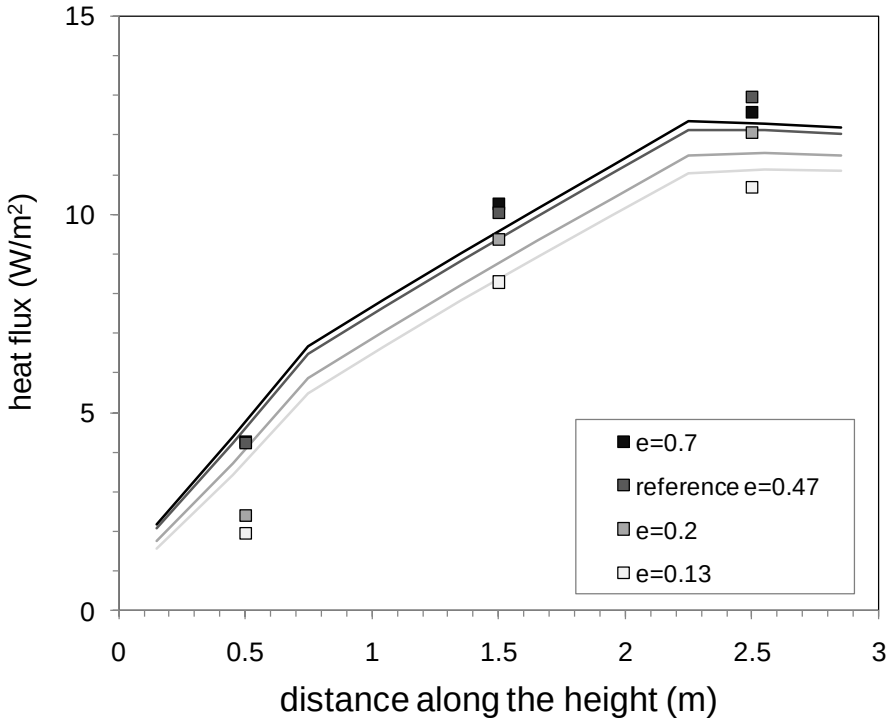
15
10
5
0
heat flux (W/m²)
0
0.5
1
1.5
2
2.5
3
distance along the height (m)
e=0.7
reference e=0.47
e=0.2
e=0.13

Figuur 11.

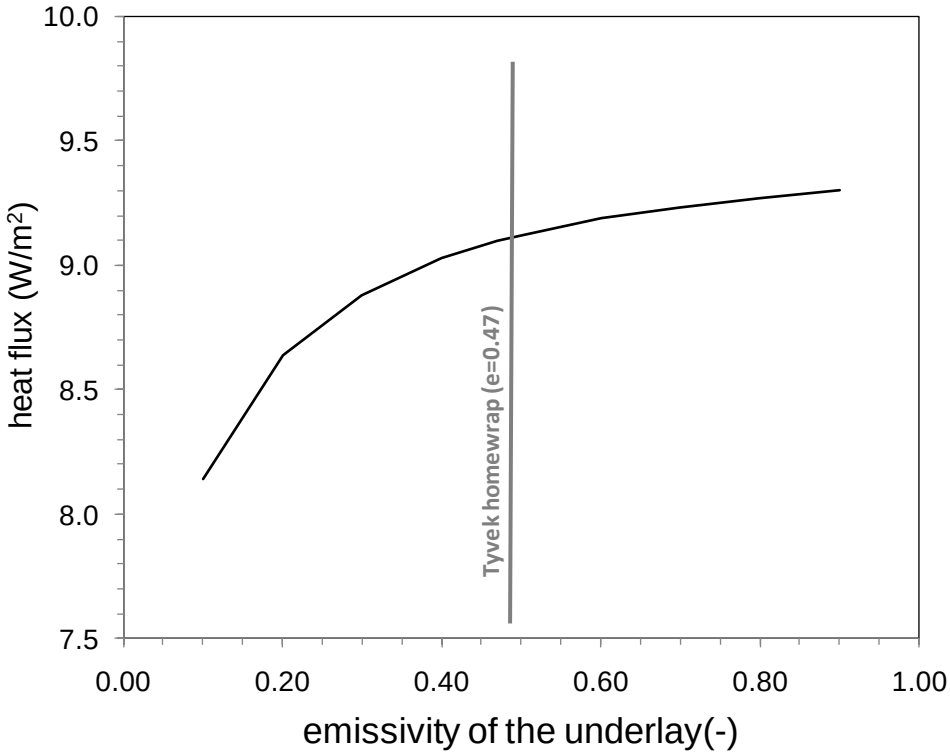
10.0
9.5
9.0
8.5
8.0
7.5
heat flux (W/m²)
Tyvek homewrap (e=0.47)
0.00
0.20
0.40
0.60
0.80
1.00
emissivity of the underlay(-)

Figure 12.

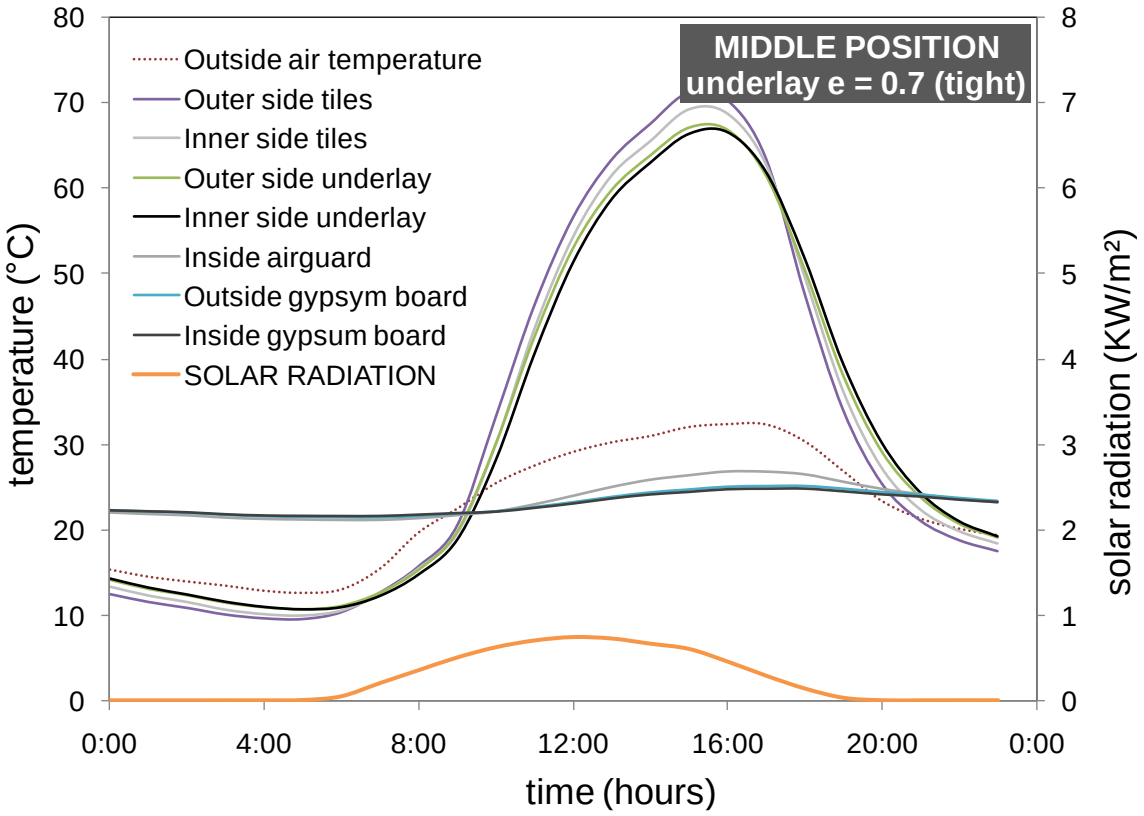
MIDDLE POSITION
underlay e = 0.7 (tight)
Outside air temperature
Outer side tiles
Inner side tiles
Outer side underlay
Inner side underlay
Inside airguard
Outside gypsym board
Inside gypsum board
SOLAR RADIATION
temperature (°C)
solar radiation (KW/m²)
time (hours)
0
10
20
30
40
50
60
70
80
0
1
2
3
4
5
6
7
8
0:00
4:00
8:00
12:00
16:00
20:00
0:00

Figure 13.

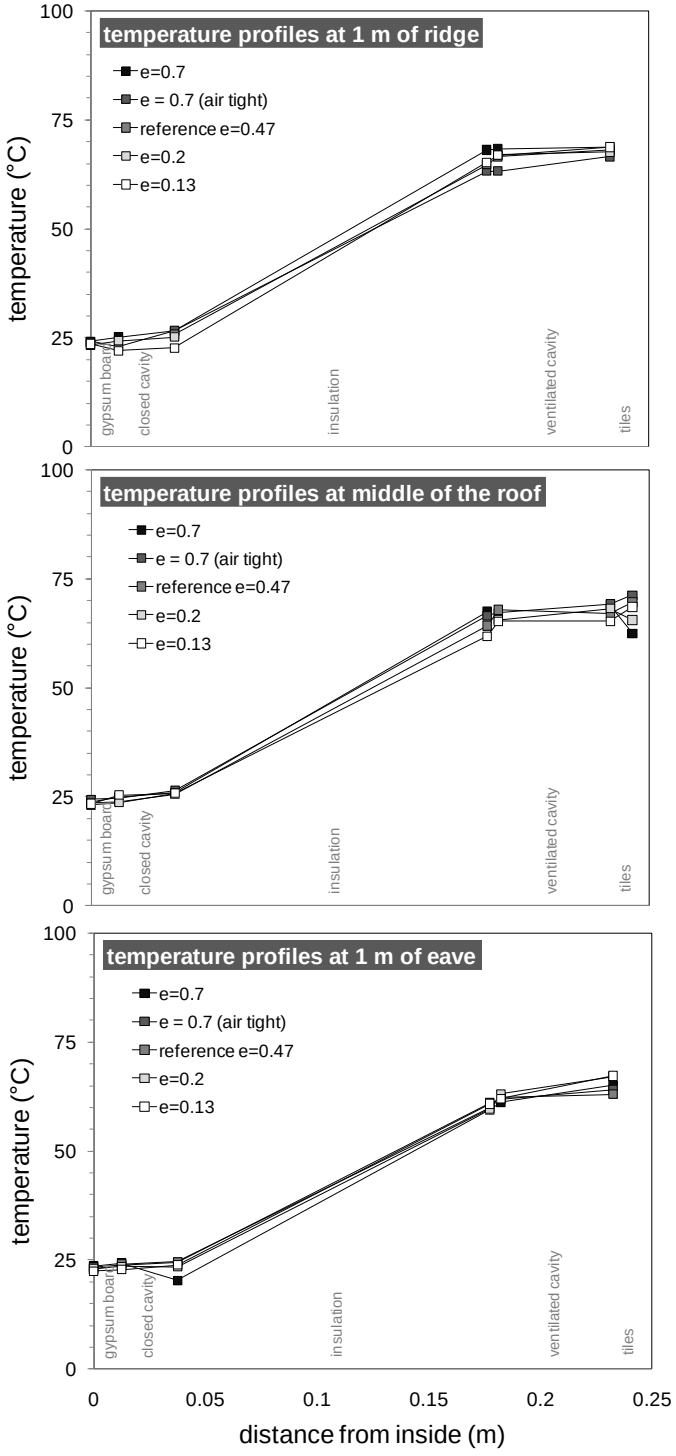
temperature profiles at 1 m of ridge
e=0.7
e = 0.7 (air tight)
reference e=0.47
e=0.2
e=0.13
temperature (°C)
100
75
50
25
0
gypsum board
closed cavity
insulation
ventilated cavity
tiles
temperature profiles at middle of the roof
e=0.7
e = 0.7 (air tight)
reference e=0.47
e=0.2
e=0.13
temperature (°C)
100
75
50
25
0
gypsum board
closed cavity
insulation
ventilated cavity
tiles
temperature profiles at 1 m of eave
e=0.7
e = 0.7 (air tight)
reference e=0.47
e=0.2
e=0.13
temperature (°C)
100
75
50
25
0
gypsum board
closed cavity
insulation
ventilated cavity
tiles
0
0.05
0.1
0.15
0.2
0.25
distance from inside (m)

Figure 14.

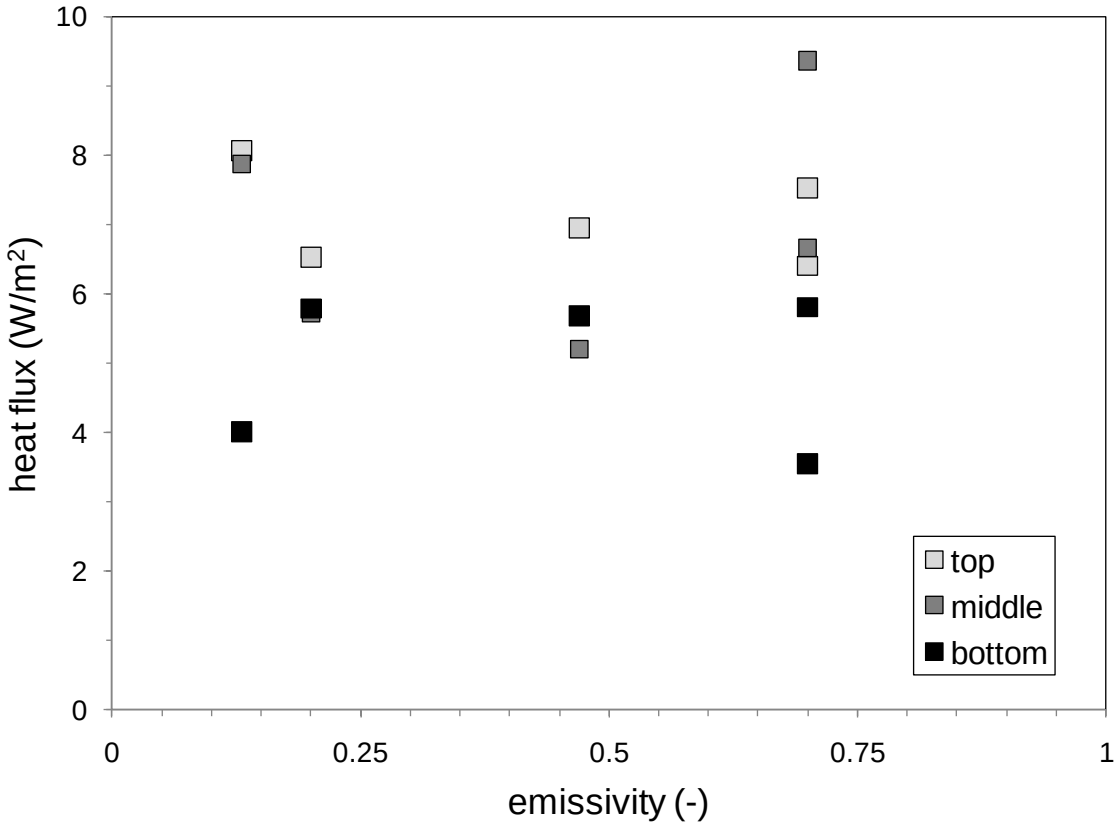
10
8
6
4
2
0
heat flux (W/m2)
0
0.25
0.5
0.75
1
emissivity (-)
top
middle
bottom

Figure 15.

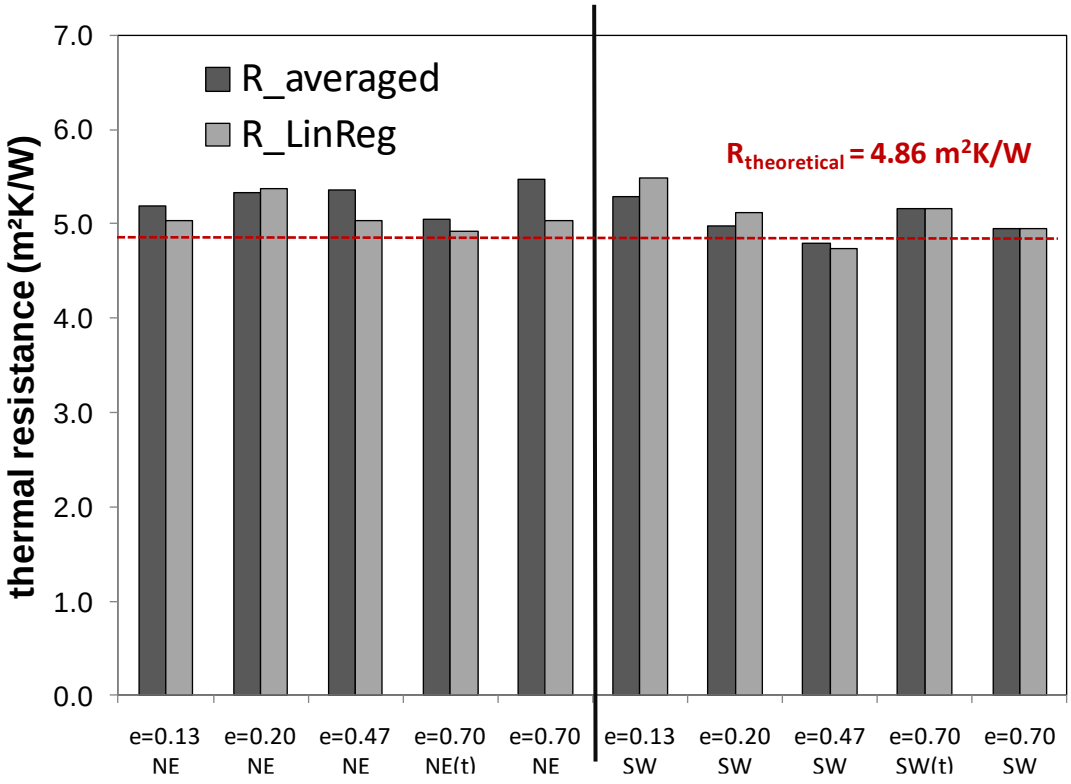
7.0
6.0
5.0
4.0
3.0
2.0
1.0
0.0
thermal resistance (m²K/W)
R_averaged
R_LinReg
R_theoretical = 4.86 m²K/W
e=0.13 NE
e=0.20 NE
e=0.47 NE
e=0.70 NE(t)
e=0.70 NE
e=0.13 SW
e=0.20 SW
e=0.47 SW
e=0.70 SW(t)
e=0.70 SW

Figure 16.

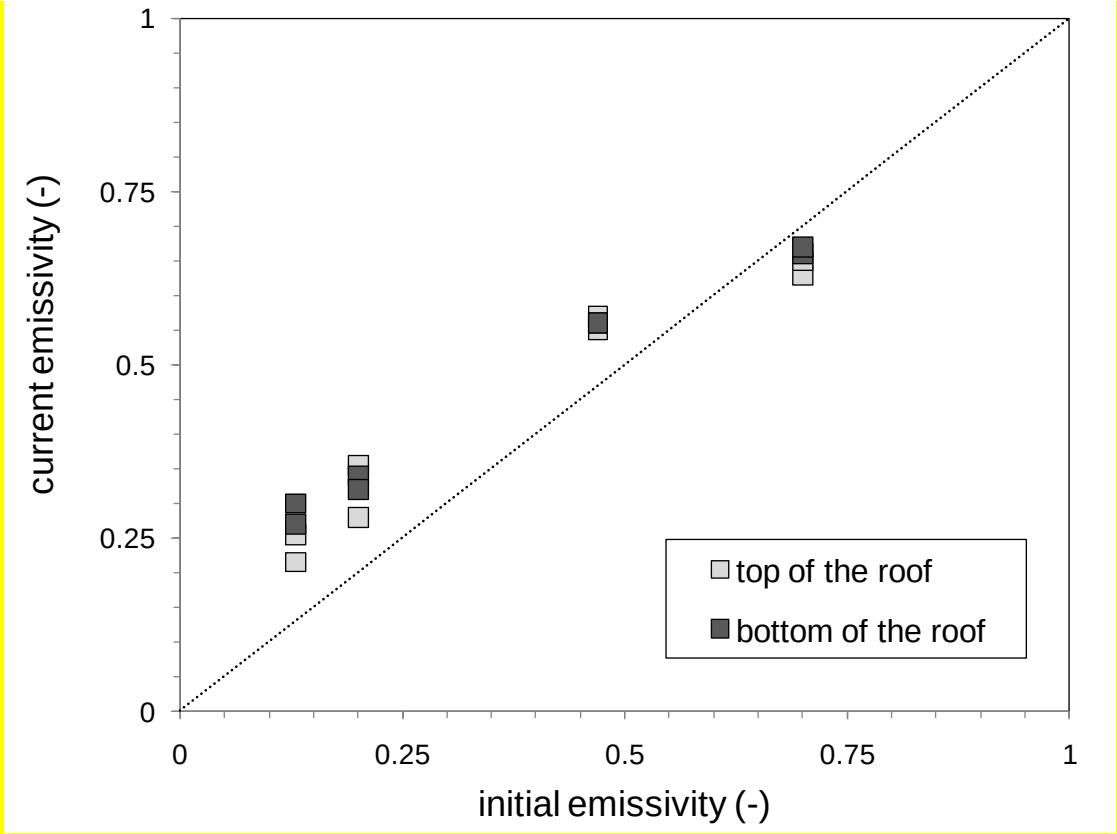
1
0.75
0.5
0.25
0
current emissivity (-)
0
0.25
0.5
0.75
1
initial emissivity (-)
top of the roof
bottom of the roof